arXiv:1601.03932v1 [physics.flu-dyn] 26 Oct 2015

Frequency downshift in a viscous fluid

J.D. Carter
email: carterj1@seattleu.edu

A. Govan
email: govana@seattleu.edu

January 18, 2016

1 Abstract

In this paper, we derive a viscous generalization of the Dysthe (1979) system from the weakly viscous generalization of the Euler equations introduced by Dias *et al.* (2008). This "viscous Dysthe" system models the evolution of a weakly viscous, nearly monochromatic wave train on deep water. It contains a term which provides a mechanism for frequency downshifting in the absence of wind and wave breaking. The equation does not preserve the spectral mean. Numerical simulations demonstrate that the spectral mean typically decreases and that the spectral peak decreases for certain initial conditions. The linear stability analysis of the plane-wave solutions of the viscous Dysthe system demonstrates that waves with wave numbers closer to zero decay more slowly than waves with wave numbers further from zero. Comparisons between experimental data and numerical simulations of the NLS, dissipative NLS, Dysthe, and viscous Dysthe systems establish that the viscous Dysthe system accurately models data from experiments in which frequency downshifting was observed *and* experiments in which frequency downshift was not observed.

2 Introduction

In the late 1970s, Lake *et al.* (1977) and Lake & Yuen (1977) conducted physical experiments that investigated the evolution of nonlinear wave trains on deep water. They found that the growth of the Benjamin-Feir instability is followed by a shift in the spectral peak to a frequency closer to zero. Subsequent experiments, including those in Su *et al.* (1982) and Melville (1982), demonstrated that the amplitude of the lower sideband grows and eventually overtakes that of the carrier wave. These later experimental studies focused on waves with larger steepness and involved wave breaking. More recently, Segur *et al.* (2005*a*) conducted similar experiments without wave breaking or wind. They found that frequency downshifting (FD) is not observed (in their tank) if the waves have "small or moderate" amplitudes and that FD is observed if the amplitude of the carrier wave is "large" or if the sideband perturbations are "large enough." They also found that if FD occurs then (i) the spectral mean (defined below)

decreases monotonically in time and (ii) FD occurs in the higher harmonics before it occurs in the fundamental. The goal of the current work is to provide a mathematical justification for FD that does not rely on wind or wave breaking. Readers interested in wind and wave-breaking justifications for FD are referred to Trulsen & Dysthe (1990); Hara & Mei (1991); Kato & Oikawa (1995); Islas & Schober (2011).

There are two quantities that are commonly used to quantify frequency downshifting: the spectral peak and the spectral mean. The spectral peak, k_p, is defined to be the wave number corresponding to the Fourier mode with largest magnitude. The spectral mean, k_m, is defined by

$$k_m = \frac{\mathcal{P}}{\mathcal{M}}, \tag{1}$$

where $\mathcal{M}$, the "mass," and $\mathcal{P}$, the "linear momentum," are defined by

$$\mathcal{M} = \frac{1}{L}\int_0^L |\eta|^2 d\xi, \tag{2a}$$

$$\mathcal{P} = \frac{i}{2L}\int_0^L \left(\eta\eta_\xi^* - \eta_\xi\eta^*\right) d\xi, \tag{2b}$$

where η and L represent the free surface displacement and period of the solution/wave train respectively. We note that while some studies use $\mathcal{P}$ by itself as a measure of FD, we focus on k_p and k_m.

Zakharov (1968) derived the cubic nonlinear Schrödinger equation (NLS) from the Euler equations as a model for the evolution of the envelope of a nearly monochromatic wave group. NLS preserves the spectral mean, so it cannot be used to model FD. Dysthe (1979) carried out the NLS perturbation analysis one order higher to obtain what is now known as the Dysthe system. Lo & Mei (1985) numerically solved NLS and the Dysthe system and established that the Dysthe system more accurately predicts the evolution of mildly sloped, narrow-banded, weakly nonlinear waves over longer time periods than does NLS. They also found that dissipative generalizations of the Dysthe system are required to model waves of moderate steepness over long distances. Finally, their numerical studies showed that the Dysthe system did not lead to a permanent FD even though the Dysthe system does not preserve the spectral mean. Segur *et al.* (2005*a*) established that the dissipative NLS equation accurately modeled the evolution of waves trains in which no FD occurred and that it cannot model FD because it preserves the spectral mean. The dissipative NLS equation was used as an ad-hoc model without formal justification until Dias *et al.* (2008) derived it from a weakly viscous generalization of the Euler equations. The first step in the current work is to carry out the Dysthe perturbation analysis starting from the Dias *et al.* (2008) weakly viscous generalization of the Euler equations in order to derive a new system which we call the viscous Dysthe system.

The paper is organized as follows. Section 3 contains the derivation of the viscous Dysthe system. Section 4 contains a summary of the main properties of this new equation. Section 5 contains comparisons of viscous Dysthe predictions with experimental data from two experiments, one of which exhibiting FD.

3 Derivation of the viscous Dysthe equation

Dias *et al.* (2008) introduced the following system for an infinitely-deep weakly viscous fluid

$$\phi_{xx} + \phi_{yy} + \phi_{zz} = 0, \qquad \text{for } -\infty < z < \eta, \tag{3a}$$

$$\phi_t + \frac{1}{2}\left|\nabla\phi\right|^2 + g\eta = -2\bar{\nu}\phi_{zz}, \qquad \text{at } z = \eta, \tag{3b}$$

$$\eta_t + \eta_x\phi_x + \eta_y\phi_y = \phi_z + 2\bar{\nu}\Delta\eta, \qquad \text{at } z = \eta, \tag{3c}$$

$$|\nabla\phi| \to 0, \qquad \text{as } z \to -\infty. \tag{3d}$$

Here $\phi = \phi(x, y, z, t)$ is the velocity potential of the fluid, $\eta = \eta(x, y, t)$ is the free-surface displacement, g is the acceleration due to gravity, and $\bar{\nu} > 0$ is the kinematic viscosity of the fluid. This model assumes that gravity and viscosity are the only external forces acting on the fluid. The Euler equations are obtained from (3) by setting $\bar{\nu} = 0$.

Substituting

$$\phi = \phi_0 \mathrm{e}^{ik_0x + k_0z - i\lambda_0 t}, \tag{4a}$$

$$\eta = \eta_0 \mathrm{e}^{ik_0x - i\lambda_0 t}, \tag{4b}$$

into the linearized version of (3) gives its linear "dispersion" relation

$$\lambda_0 = \pm\sqrt{gk_0} - 2ik_0^2\bar{\nu}. \tag{5}$$

The $\pm\sqrt{gk_0}$ term represents dispersion while the $-2ik_0^2\bar{\nu}$ term represents (wave-number dependent) dissipation. This establishes that, according to this model, small-amplitude waves with large wave number will decay faster than small-amplitude waves with small wave number.

Following the work of Dysthe (1979), assume

$$\eta(x, y, t) = \epsilon^3\bar{\eta} + \epsilon B\mathrm{e}^{ik_0x - i\omega_0 t} + \epsilon^2 B_2\mathrm{e}^{2(ik_0x - i\omega_0 t)} + \cdots + c.c., \tag{6a}$$

$$\phi(x, y, z, t) = \epsilon^2\bar{\phi} + \epsilon A_1\mathrm{e}^{k_0z + ik_0x - i\omega_0 t} + \epsilon^2 A_2\mathrm{e}^{2(k_0z + ik_0x - i\omega_0 t)} + \cdots + c.c., \tag{6b}$$

where k_0 is a positive constant and $\epsilon = a_0k_0 \ll 1$ is a small dimensionless parameter. Here a_0 represents a typical amplitude, k_0 represents the wave number of the carrier wave, and *c.c.* stands for complex conjugate. The A's and $\bar{\phi}$ depend on the slow variables $X = \epsilon x$, $Y = \epsilon Y$, $Z = \epsilon x$, and $T = \epsilon t$, while the B's and $\bar{\eta}$ depend on X, Y and T. Although it is done without loss of generality, assuming $k_0 > 0$ is significant because it determines the form of the z dependence in ϕ. Next, assume

$$A_j = A_{j0} + \epsilon A_{j1} + \epsilon^2 A_{j2} + \epsilon^3 A_{j3} + \ldots, \qquad \text{for } j = 1, 2, 3, \ldots, \tag{7a}$$

$$B_j = B_{j0} + \epsilon B_{j1} + \epsilon^2 B_{j2} + \epsilon^3 B_{j3} + \ldots, \qquad \text{for } j = 2, 3, 4, \ldots, \tag{7b}$$

$$\bar{\eta} = \bar{\eta}_0 + \epsilon\bar{\eta}_1 + \epsilon^2\bar{\eta}_2 + \ldots, \tag{7c}$$

$$\bar{\phi} = \bar{\phi}_0 + \epsilon\bar{\phi}_1 + \epsilon^2\bar{\phi}_2 + \ldots. \tag{7d}$$

Following the work of Dias *et al.* (2008), assume that viscosity effects are small by assuming $\bar{\nu} = \epsilon^2\nu$. Substituting (6)-(7) into (3) and carrying out the perturbation analysis through $\mathcal{O}(\epsilon^4)$ gives the deep-water dispersion relationship,

$$\omega_0^2 = gk_0, \tag{8}$$

the system that defines B and $\bar{\phi}_0$,

$$\begin{aligned} &2i\omega_0\big(B_T + \frac{g}{2\omega_0}B_X\big) + \epsilon\Big(- \frac{g}{4k_0}B_{XX} + \frac{g}{2k_0}B_{YY} - 4gk_0^3|B|^2B + 4ik_0^2\nu B\Big) \\ &\quad + \epsilon^2\Big(- i\frac{g}{8k_0^2}B_{XXX} + i\frac{3g}{4k_0^2}B_{XYY} + 2igk_0^2B^2B_X^* \\ &\qquad + 12igk_0^2|B|^2B_x - 2k_0\omega_0B\bar{\phi}_{0X} + 8k_0\omega_0\nu B_X\Big) = 0, \ \text{ at } Z = 0, \end{aligned} \tag{9a}$$

$$\bar{\phi}_{0Z} = 2\omega_0\Big(|B|^2\Big)_X, \qquad \text{at } Z = 0, \tag{9b}$$

$$\bar{\phi}_{0XX} + \bar{\phi}_{0ZZ} = 0, \qquad \text{for} - \infty < Z < 0, \tag{9c}$$

$$\bar{\phi}_{0Z} \to 0, \qquad \text{as } Z \to -\infty, \tag{9d}$$

and

$$B_2 = k_0B^2 + \mathcal{O}(\epsilon), \tag{10a}$$

$$B_3 = \frac{3}{2}k_0^2B^3 + \mathcal{O}(\epsilon). \tag{10b}$$

Equations (10a) and (10b) define the leading-order contributions to the amplitudes of the second and third harmonics of the carrier wave respectively. Following a similar procedure, but solving for the leading-order term of the velocity potential instead of the leading-order term of the surface displacement, gives

$$\begin{aligned} &2i\omega_0\big(A_T + \frac{g}{2\omega_0}A_X\big) + \epsilon\Big(- \frac{g}{4k_0}A_{XX} + \frac{g}{2k_0}A_{YY} - 4k_0^4|A|^2A + 4ik_0^2\nu A\Big) \\ &\quad + \epsilon^2\Big(- i\frac{g}{8k_0^2}A_{XXX} + i\frac{3g}{4k_0^2}A_{XYY} - 2ik_0^3A^2A_X^* \\ &\qquad + 12ik_0^3|A|^2A_x - 2k_0\omega_0A\bar{\phi}_{0X} + 8k_0\omega_0\nu A_X\Big) = 0, \ \text{ at } Z = 0, \end{aligned} \tag{11a}$$

$$\bar{\phi}_{0Z} = \frac{2k_0^2}{\omega_0}\Big(|A|^2\Big)_X, \qquad \text{at } Z = 0, \tag{11b}$$

$$\bar{\phi}_{0XX} + \bar{\phi}_{0ZZ} = 0, \qquad \text{for} - \infty < Z < 0, \tag{11c}$$

$$\bar{\phi}_{0Z} \to 0, \qquad \text{as } Z \to -\infty. \tag{11d}$$

The systems in (9) and (11) are related by

$$B = \frac{ik_0}{\omega_0}A + \epsilon\frac{1}{2\omega_0}A_X + \epsilon^2\Big(\frac{i}{8k_0\omega_0}A_{XX} - \frac{i}{4k_0\omega_0}A_{YY} + \frac{ik_0^4}{2g\omega_0}|A|^2A\Big) + \mathcal{O}(\epsilon^3), \tag{12a}$$

$$A = -\frac{i\omega_0}{k_0}B + \epsilon\frac{\omega_0}{2k_0^2}B_X + \epsilon^2\Big(\frac{3i\omega_0}{8k_0^3}B_{XX} - \frac{i\omega_0}{4k_0^3}B_{YY} + \frac{ik_0\omega_0}{2}|B|^2B\Big) + \mathcal{O}(\epsilon^3). \quad (12b)$$

We now change variables in order to enter into a coordinate frame moving with the linear group velocity, $c_g = \frac{\omega_0}{2k_0}$. For simplicity, we also assume that there is no Y dependence. Let

$$B(X,Y,T) = \tilde{B}(\xi,\chi), \quad (13a)$$

$$A(X,Y,Z,T) = \frac{\omega_0}{k_0}\tilde{A}(\xi,\chi,\zeta), \quad (13b)$$

$$\bar{\phi}_0(X,Y,Z,T) = 4\omega_0\tilde{\Phi}(\xi,\chi,\zeta), \quad (13c)$$

$$\nu = \frac{\omega_0}{4k_0^2}\delta, \quad (13d)$$

$$\chi = \epsilon k_0 X, \quad (13e)$$

$$\xi = 2k_0X - \omega_0 T, \quad (13f)$$

$$\zeta = k_0 Z. \quad (13g)$$

This change of variables leads to (where tildes have been dropped for convenience)

$$iB_\chi - B_{\xi\xi} - 4k_0^2|B|^2B + i\delta B + \epsilon\big(8ik_0^2B^2B_\xi^* + 32ik_0^2|B|^2B_\xi - 16k_0^2B\Phi_\xi + 5\delta B_\xi\big) = 0, \text{ at } \zeta = 0, \quad (14a)$$

$$\Phi_\zeta = \Big(|B|^2\Big)_\xi, \qquad \text{at } \zeta = 0, \quad (14b)$$

$$4\Phi_{\xi\xi} + \Phi_{\zeta\zeta} = 0, \qquad \text{for } -\infty < \zeta < 0, \quad (14c)$$

$$\Phi_\zeta \to 0, \qquad \text{as } \zeta \to -\infty, \quad (14d)$$

and

$$iA_\chi - A_{\xi\xi} - 4k_0^2|A|^2A + i\delta A + \epsilon\big(32ik_0^2|A|^2A_\xi - 16k_0^2A\Phi_\xi + 5\delta A_\xi\big) = 0, \text{ at } \zeta = 0, \quad (15a)$$

$$\Phi_\zeta = \big(|A|^2\big)_\xi, \qquad \text{at } \zeta = 0, \quad (15b)$$

$$4\Phi_{\xi\xi} + \Phi_{\zeta\zeta} = 0, \qquad \text{for } -\infty < \zeta < 0, \quad (15c)$$

$$\Phi_\zeta \to 0, \qquad \text{as } \zeta \to -\infty. \quad (15d)$$

We call the systems given in equations (14) and (15) the viscous Dysthe system for the surface displacement (the vB system) and the viscous Dysthe system for the velocity potential (the vA system) respectively. These equations, which describe the evolution of a narrow-banded, weakly nonlinear, weakly viscous fluid and (as shown below) accurately predict FD, are the main results of this paper. NLS is obtained from equation (14a) or (15a) by setting $\delta = \epsilon = 0$. The classical Dysthe systems for the surface displacement and velocity potential are obtained from (14) and (15) by setting $\delta = 0$.

It is important to note that there is only one free parameter in the viscous Dysthe systems. This parameter, δ, is empirically determined by fitting the decay of $\mathcal{M}$. This will establish (see below) that changes in $\mathcal{M}$, $\mathcal{P}$, and k_m are all determined by δ. This is qualitatively different from other FD models that have two (or more) free parameters that can be used to fit the decay of both $\mathcal{M}$ and $\mathcal{P}$.

4 Properties of the viscous Dysthe system

4.1 Mass and linear momentum

Trulsen & Dysthe (1997) showed that the Dysthe system for the velocity potential (the vA system with $\delta = 0$) preserves both $\mathcal{M}$ and $\mathcal{P}$ in χ while the Dysthe system for the surface displacement (the vB system with $\delta = 0$) preserves $\mathcal{M}$, but not $\mathcal{P}$. Moreover, they established that the sign of $\mathcal{P}_\chi$ in the vB system with $\delta = 0$ is not definite and therefore the Dysthe system can predict frequency upshifting. Lo & Mei (1985) conducted numerical studies of the vB system with $\delta = 0$ and did not observe a permanent downshift in any of their simulations. These results suggest that the $B^2 B^*_\xi$ term (the only term that differentiates the vA and vB systems when $\delta = 0$) is not the mechanism for FD.

We note that the vA system with $\delta = 0$ is Hamiltonian while the vB system with $\delta = 0$ is likely not Hamiltonian (see Carter, 2001; Segur *et al.*, 2005*b*). Gramstad & Trulsen (2011) derived a Hamiltonian generalization of the Dysthe system for the surface displacement. Although we do not study this equation here, we expect that the results shown below will generalize to it because the $\mathcal{O}(\epsilon)$ viscosity term, $5\epsilon\delta B_\xi$, provides the mechanism for FD.

The χ dependences of $\mathcal{M}$ and $\mathcal{P}$ in the vB system are given by

$$\mathcal{M}_\chi = -2\delta\mathcal{M} - 10\epsilon\delta\mathcal{P}, \tag{16a}$$

$$\mathcal{P}_\chi = -2\delta\mathcal{P} - 10\epsilon\delta\mathcal{Q} - 16\epsilon k_0^2\mathcal{R}, \tag{16b}$$

where

$$\mathcal{Q} = \frac{1}{L}\int_0^L |B_\xi|^2 d\xi, \tag{17a}$$

$$\mathcal{R} = \mathrm{Re}\left(\frac{1}{L}\int_0^L |B|^2 B B^*_{\xi\xi} d\xi\right). \tag{17b}$$

Further

$$\left(k_m\right)_\chi = \left(\frac{\mathcal{P}}{\mathcal{M}}\right)_\chi = -\frac{10\epsilon\delta}{\mathcal{M}^2}\left(\mathcal{M}\mathcal{Q} - \mathcal{P}^2\right) - 16\epsilon k_0^2\frac{\mathcal{R}}{\mathcal{M}}. \tag{18}$$

The Cauchy-Schwarz inequality establishes that $(\mathcal{M}\mathcal{Q} - \mathcal{P}^2) > 0$. This suggests that the vB system will exhibit FD in the spectral mean sense. However, the sign of $\mathcal{R}$ can vary, so FD is not necessarily guaranteed. Note that FD is guaranteed in the vA system because the $\mathcal{R}$ term is not involved. FD does not occur in either the vA or the vB system if either i) $\delta = 0$ (i.e. $\nu = 0$) or ii) $\epsilon = 0$ (not

physically interesting). Finally, equation (18) establishes that FD is a higher-order effect, corroborating the Segur *et al.* (2005*a*) result that the dissipative NLS equation preserves the spectral mean.

4.2 Plane-Wave Solutions

Consider solutions of the vB system with the following form

$$B(\xi,\chi) = B_0 \exp\big(il\xi + w_r(\chi) + iw_i(\chi) + i\rho\big), \tag{19}$$

where B_0, l, and ρ are real constants and w_r and w_i are real-valued functions. This gives

$$\Phi(\xi,\chi,\zeta) = 0, \tag{20a}$$

$$w_r' + \delta(1+5\epsilon l) = 0, \tag{20b}$$

$$w_i' - l^2 + 4B_0^2k_0^2(1+6\epsilon l)\mathrm{e}^{2w_r} = 0. \tag{20c}$$

The parameter ρ does not play a role in the ODEs that define ω_r and ω_i because of the gauge invariance of the vB system. This allows all complex B_0 to be considered by assuming, without loss of generality, that B_0 is a positive constant. The solution of this system is

$$w_r(\chi) = -\delta(1+5\epsilon l)\chi, \tag{21a}$$

$$w_i(\chi) = l^2\chi + \frac{2A_0^2k_0^2(1+6\epsilon l)}{\delta(1+5\epsilon l)}\Big(\mathrm{e}^{-2\delta(1+5\epsilon l)\chi} - 1\Big). \tag{21b}$$

The constants of integration were chosen so that these (viscous) solutions limit to the solutions of the (nonviscous) Dysthe system in the $\delta \to 0$ limit. Note that (21a) establishes that if $\delta > 0$, then to leading order all plane-wave solutions of the vB system decay to zero as $\chi \to \infty$. Just as in NLS and the Dysthe system, choosing $l \neq 0$ corresponds to shifting the wave number of the carrier wave. The function ω_r depends on l in such a way that it takes into account the correct (up to the order of the equation) rate of dissipation for the shifted carrier wave (see equations (5) and (13)). Therefore, we assume $l = 0$ for the remainder of the paper.

4.3 Linear stability analysis

In order to study the stability of solutions of the form given in equation (19), we consider perturbed solutions of the form

$$B_{\mathrm{pert}}(\xi,\chi) = \big(B_0 + \mu u(\xi,\chi) + i\mu v(\xi,\chi)\big)\exp\big(w_r(\chi) + iw_i(\chi)\big), \tag{22a}$$

$$\Phi_{\mathrm{pert}}(\xi,\chi,\zeta) = 0 + \mu p(\xi,\chi,\zeta), \tag{22b}$$

where μ is a small real parameter; u, v, and p are real-valued functions; and $w_r(t)$ and $w_i(t)$ are given in equation (21). Note that the decay due to $w_r(t)$

has been factored out in equation (22a). This allows the evolution of the perturbation, $u + iv$, to be directly compared to the constant B_0. If u and/or v grow without bound in χ, we say that the solutions is linearly unstable (even though the magnitude of the entire perturbed solution may decay to zero).

Substituting (22) into (14), linearizing in μ, and separating into real and imaginary parts leads to a system of coupled PDEs that have constant coefficients in ξ and ζ. Without loss of generality, assume

$$u(\xi,\chi) = U(\chi)\mathrm{e}^{iq\xi} + U^*(\chi)\mathrm{e}^{-iq\xi}, \tag{23a}$$

$$v(\xi,\chi) = V(\chi)\mathrm{e}^{iq\xi} + V^*(\chi)\mathrm{e}^{-iq\xi}, \tag{23b}$$

$$p(\xi,\chi,\zeta) = \mathrm{sign}(q)B_0\big(iU(\chi)\mathrm{e}^{iq\xi} - iU^*(\chi)\mathrm{e}^{-iq\xi}\big)\mathrm{e}^{2|q|\zeta}\mathrm{e}^{-2\delta\chi}, \tag{23c}$$

where q is a real constant, and U and V are complex-valued functions. The form for p was selected because it satisfies Laplace's equation and the bottom boundary condition. Substituting (23) into the PDEs gives

$$\begin{pmatrix} U \\ V \end{pmatrix}' = \left(\mathbf{A_1} + \mathrm{e}^{-2w_r(\chi)}\mathbf{A_2}\right)\begin{pmatrix} U \\ V \end{pmatrix}, \tag{24}$$

where prime means derivative with respect to χ and $\mathbf{A_1}$ and $\mathbf{A_2}$ are the constant matrices given by

$$\mathbf{A_1} = \begin{pmatrix} 0 & -q^2 - 5i\epsilon\delta q \\ q^2 + 5i\epsilon\delta q & 0 \end{pmatrix}, \tag{25a}$$

$$\mathbf{A_2} = \begin{pmatrix} -40i\epsilon q k_0^2 & 0 \\ -8k_0^2(1-2\epsilon|q|) & -24i\epsilon q k_0^2 \end{pmatrix}. \tag{25b}$$

To our knowledge, an exact solution of (24) is not known. However, $\mathbf{A}_1$ determines the large-χ behavior of the solution because the χ dependent term is integrable on $\chi \in [0,\infty)$ (see Coddington & Levinson, 1955). The eigenvalues of $\mathbf{A_1}$ are

$$\lambda_{A_1} = \pm iq^2 \mp 5\epsilon\delta q. \tag{26}$$

This establishes that the long-term solution of (24) is given by

$$\begin{pmatrix} U \\ V \end{pmatrix} = \begin{pmatrix} -ic_1 & ic_2 \\ c_1 & c_2 \end{pmatrix}\begin{pmatrix} \exp\left((-iq^2 + 5\epsilon\delta q)\chi\right) \\ \exp\left((iq^2 - 5\epsilon\delta q)\chi\right) \end{pmatrix}, \tag{27}$$

where c_1 and c_2 are the constants of integration. Substituting this back into equation (23) gives

$$B_{\mathrm{pert}} = \Big(B_0 + 2ic_1\exp\left(i(-q\xi+q^2\chi)+5\epsilon\delta q\chi\right) + 2ic_2\exp\left(i(q\xi+q^2\chi)-5\epsilon\delta q\chi\right)\Big)\mathrm{e}^{w_r(\chi)+iw_i(\chi)}. \tag{28}$$

Observations:

- If $\delta > 0$ and $q \neq 0$, then $\mathbf{A}_1$ has an eigenvalue with positive real part. Therefore all plane-wave solutions of the vB system are linearly unstable. The growth rate of the instability is $5\epsilon\delta|q|$. This instability is not a Benjamin-Feir-like instability because *all* spatially dependent perturbations lead to exponential growth. This instability is similar to the "enhanced Benjamin-Feir" instabilities that arise in other dissipative generalizations of NLS (see Bridges & Dias, 2007; Carter & Contreras, 2008).

- If q is positive, then the c_1 term in (28) grows exponentially in χ while the c_2 term decays exponentially in χ. If q is negative, then the c_2 term grows while the c_1 term decays. This intrinsic preference for perturbations with negative wave numbers suggests FD.

- In order to make statements about the physical surface displacement, one needs to transform back into physical coordinates by using equations (6), (12), and (13). The amplitude of the carrier wave (the mode with wave number $k_0 > 0$) decays exponentially. The amplitude of the upper sideband (the mode with wave number $k_0 + |q|$) decays more rapidly than the amplitude of the carrier wave. The amplitude of the lower sideband ($k_0 - |q|$) decays more slowly than does the amplitude of the carrier wave. This suggests FD.

- In equation (28) the decay due to ω_r, namely $\exp(-\delta\chi)$, has been factored out. This decay is an $\mathcal{O}(1)$ effect, while the growth of the instability is an $\mathcal{O}(\epsilon)$ effect. This means that the decay typically dominates the growth. However, some modes decay more slowly than others. Waves with physical wave numbers closer to zero decay more slowly than those with wave numbers further from zero. This suggests FD.

- These results apply to B in (6). Calculations for the B^* term in (6) establish that the amplitude of the mode with wave number $-k_0 - |q|$ decays more rapidly than the amplitude of the carrier wave while the mode with wave number $-k_0 + |q|$ decays less rapidly. This suggests FD.

- The growth rate $5\epsilon\delta|q|$ and equation (10) establish that the instability in the second sideband grows twice as fast as the instability in the fundamental. This suggests that FD will be observed in the higher harmonics before it is observed in the fundamental (just as was observed by Segur *et al.* (2005*a*)).

5 Comparisons with experiments

In this section the validity of the vB system is tested by comparing its predictions with measurements from two physical experiments of one-dimensional, nearly monochromatic wave trains on deep water and predictions from the NLS, dissipative NLS, and Dysthe equations. The waves were created by a plunger-type wave maker that oscillates vertically at one end of a 43-foot long and 10-inch

wide wave channel. Time series were collected by eleven or twelve (depending on the experiment) wave gauges located $128+50(n-1)$cm from the wave maker were $n = 1, \ldots, 12$. The tank was long enough that reflections off the far wall did not play a role.

The first experiment examines the evolution of a nearly monochromatic wave train formed by a carrier wave perturbed by sidebands of "moderate" amplitude. The second experiment examines the evolution of a nearly monochromatic wave train formed by a very similar carrier wave perturbed by sidebands of "large" amplitude. FD was observed in the second experiment, but not the first. For each experiment, the wave gauges recorded time series lasting 23.4033 seconds. The experimental initial conditions were comprised of a carrier wave with a frequency of 3.33Hz ($k_0 = 0.447475\text{cm}^{-1}$) and one upper and one lower seeded sideband each separated from the carrier wave by 0.17092Hz ($\Delta k = 0.04273\text{cm}^{-1}$). Complete experimental details are found in Section 6 of Segur *et al.* (2005*a*).

All equations were solved numerically by assuming periodic boundary conditions and using split-step pseudospectral methods that allow the linear parts of the PDEs to be solved exactly in Fourier space. The initial conditions for the PDEs were

$$B(\xi, \chi = 0) = \sum_{n=-3}^{3} \frac{1}{\epsilon} a_n^* \, \mathrm{e}^{in\xi/(78\epsilon)}. \tag{29}$$

This form was selected for the initial conditions because it contains all of the modes with significant amplitude measured by the first wave gauge. The complex conjugates of the amplitudes were used because of the change of variables in equation (13f). Note that when solving the NLS or dissipative NLS equation, ϵ is set to zero in equation (14a) in order to determine the correct equation and then a value of ϵ from either Table 1 or 2 was used in (29) to obtain the appropriately scaled initial condition.

5.1 Moderate-amplitude experiment

Table 1 contains the values of the physical parameters for this experiment. Figure 1 contains plots of the Fourier amplitudes (in centimeters) versus x, the distance from the first wave gauge (in centimeters). Unlike the plots in Segur *et al.* (2005*a*), the experimental data here are not scaled. Although the amplitudes of the sidebands increase, the amplitude of the carrier wave is dominant at all measurement sites. This means that FD in the spectral peak sense did not occur in this experiment.

The dissipative theories (viscous Dysthe and dissipative NLS) do a much better job predicting the evolution of the amplitudes of the carrier wave and the six nearest sidebands than do the conservative theories (NLS and Dysthe). Both conservative models greatly over predict the growth of the sidebands. The vB system provides predictions for all seven amplitudes that are at least as accurate as, if not more accurate than, the predictions given by the dissipative NLS equation. For this experiment, the vA system (results not shown) provides predictions that are approximately the same as the vB predictions.

parameter	symbol	value
wave number of carrier wave	k_0	0.447475
initial amplitude of carrier wave	a_0	0.057756+0.091504i
initial amplitude of first upper sideband	a_1	0.0093077-0.013313i
initial amplitude of second upper sideband	a_2	-0.0028183-0.0010747i
initial amplitude of third upper sideband	a_3	-0.00025316+0.00037694i
initial amplitude of first lower sideband	a_{-1}	0.0035254-0.013840i
initial amplitude of second lower sideband	a_{-2}	0.00033989+0.0024345i
initial amplitude of third lower sideband	a_{-3}	0.00036841+0.00020832i
dimensionless parameter	$\epsilon = 2k_0\|a_0\|$	0.096840
viscosity coefficient	δ	0.0011068

Table 1: Experimental parameters for the moderate-amplitude experiment.

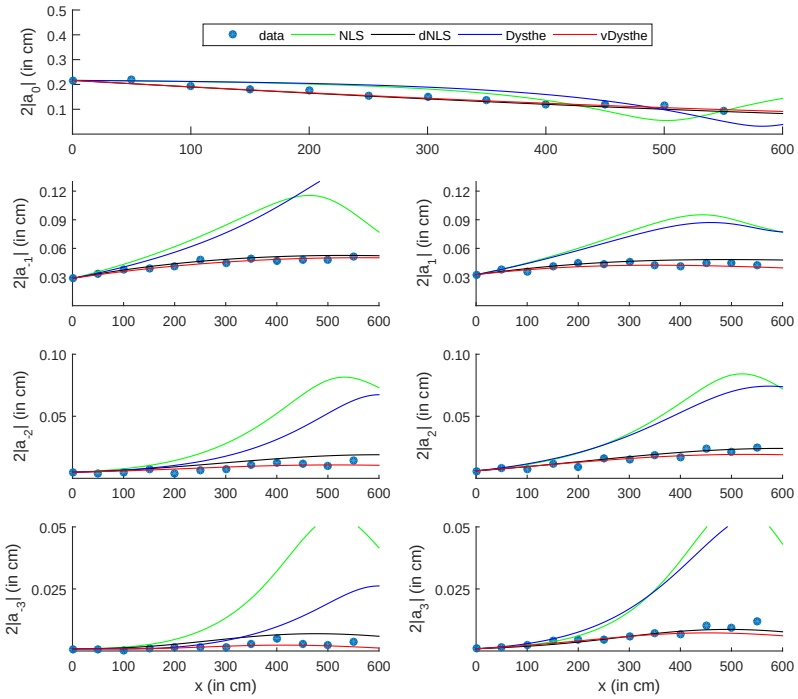

Figure 1: Plots of the amplitudes (in cm) of the carrier wave and the six nearest sidebands plotted versus the distance (in cm) from the first wave gauge for the moderate-amplitude experiment.

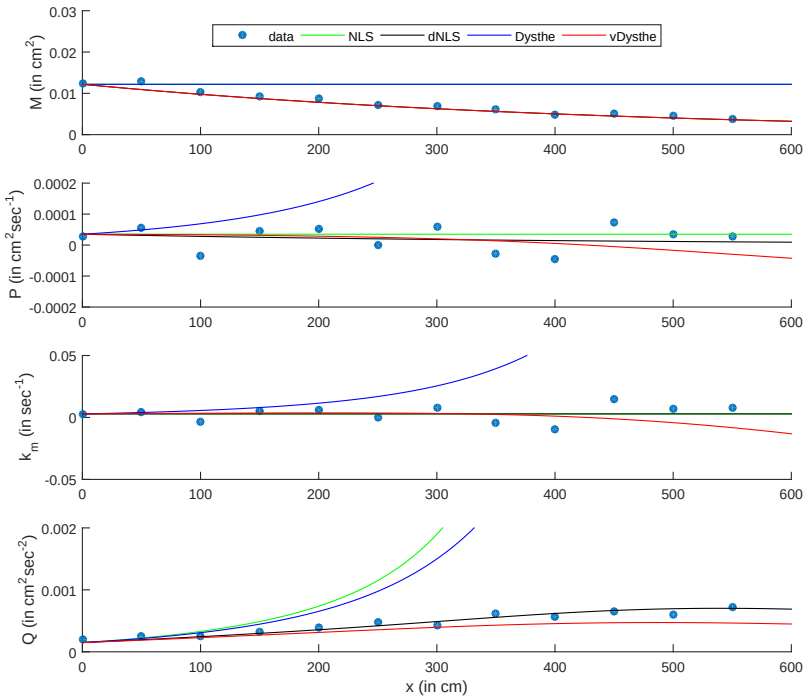

Figure 2: Plots of $\mathcal{M}$, $\mathcal{P}$, k_m, and $\mathcal{Q}$ versus the distance (in cm) from the first wave gauge for the moderate-amplitude experiment.

Figure 2 shows how the quantities $\mathcal{M}$, $\mathcal{P}$, k_m, and $\mathcal{Q}$ evolved as the wave train progressed down the tank. The spectral mean, k_m, is constant to within experimental error and therefore FD in the spectral mean sense did not occur in this experiment. The leading-order in ϵ versions of equations (16) establish that (to leading order) $\mathcal{M}$ decays exponentially. Using an exponential best fit empirically determines the only free parameter in the system, $\delta = 0.001107\text{cm}^{-1}$.

The dissipative theories do a much better job predicting the evolution of $\mathcal{M}$ and $\mathcal{Q}$ than do the conservative theories. The Dysthe equation predicts large increases in $\mathcal{P}$ and k_m that were not observed in the experiment. It is not possible to determine which of the other models provides the best prediction for these quantities because the changes are within the bounds of experimental measurement error. However, we note that the vB system predicts a small FD and hypothesize that FD may have been observed had the experimental tank been longer.

parameter	symbol	value
wave number of carrier wave	k_0	0.447475
initial amplitude of carrier wave	a_0	-0.057134+0.088094i
initial amplitude of first upper sideband	a_1	0.00092806-0.034102i
initial amplitude of second upper sideband	a_2	0.0069104+0.014365i
initial amplitude of third upper sideband	a_3	-0.0036015-0.0027146i
initial amplitude of first lower sideband	a_{-1}	0.010223+0.033383i
initial amplitude of second lower sideband	a_{-2}	0.0088658+0.0016430i
initial amplitude of third lower sideband	a_{-3}	-0.0014867-0.0013086i
dimensionless parameter	$\epsilon = 2k_0\|a_0\|$	0.093970
viscosity coefficient	δ	0.0012697

Table 2: Experimental parameters for the large-amplitude experiment.

5.2 Large-amplitude experiment

Table 2 contains the values of the physical parameters for this experiment. Figure 3 contains plots of the Fourier amplitudes for this experiment. In this experiment, the amplitude of the first lower sideband overtakes that of the carrier wave somewhere between 300 and 350cm from the first wave gauge. Therefore FD in the spectral peak sense occurred in this experiment.

The vB system provides the most accurate prediction for the evolution for all amplitudes. It does a good job predicting the evolution of all seven amplitudes. The vB system predicts that the amplitude of the first lower sideband will overtake that of the carrier wave approximately 223cm from the first wave gauge. This is earlier than what was observed in the experiment and is related to the fact that the vB system slightly over predicts the amplitude of the first lower sideband. Regardless, the vB system qualitatively predicts the evolution of the wave train. The vA system provides predictions (results not shown) that are noticeably less accurate than those of the vB system. We note that the accuracy of the vB system comes from a combination of the higher-order viscous term and the higher-order nonlinear terms. Predictions from the NLS equation with the two viscous terms added are much less accurate than those from the vB system.

Figure 4 shows how the quantities $\mathcal{M}$, $\mathcal{P}$, k_m, and $\mathcal{Q}$ evolved as the wave train progressed down the tank for the large-amplitude experiment. The spectral mean, k_m, decreases substantially and therefore FD in the spectral mean sense occurred in this experiment. An exponential fit of the experimental $\mathcal{M}$ data establishes that $\delta = 0.0012697\text{cm}^{-1}$.

The vB system provides the best predictions for all four of these quantities. It predicts a brief temporary frequency upshift followed by a downward trend. The Dysthe equation predicts a temporary, but dramatic, frequency upshift that is quite different than what was experimentally observed. Both the NLS and dissipative NLS predict that k_m is constant even though the experimental data shows a definite downward trend. Note that the plots of $\mathcal{P}$ and k_m make

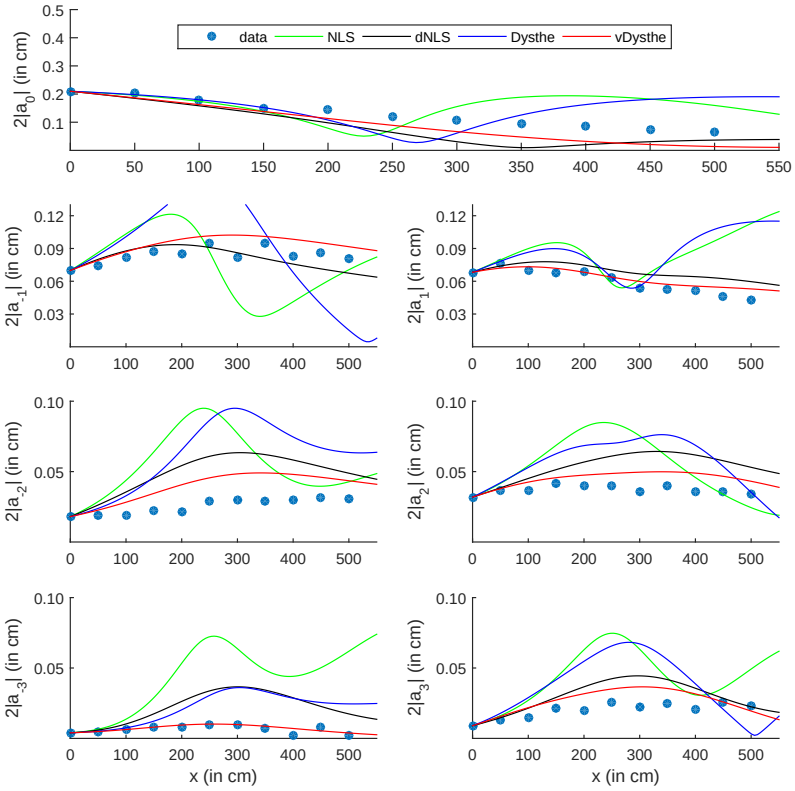

Figure 3: Plots of the amplitudes (in cm) of the carrier wave and the six nearest sidebands plotted versus the distance (in cm) from the first wave gauge for the large-amplitude experiment.

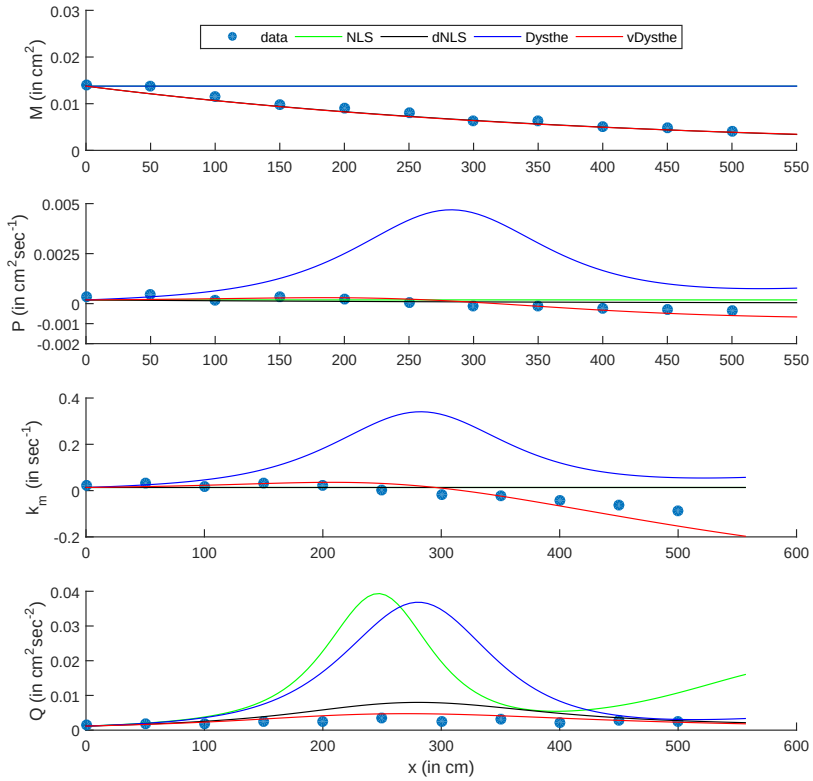

Figure 4: Plots of $\mathcal{M}$, $\mathcal{P}$, k_m, and $\mathcal{Q}$ versus the distance (in cm) from the first wave gauge for the large-amplitude experiment.

it obvious that the initial conditions used in the numerical simulations of the PDEs do not exactly match the experimental initial conditions. This is because only the carrier wave and the first six sidebands are used in the initial conditions (see equation (29)). If more modes are included, the initial points line up more closely, but the qualitative behavior of the plots remains the same.

We are grateful to Shusen Ding, Diane Henderson, and Harvey Segur for helpful discussions. This material is based upon work supported by the National Science Foundation under grant DMS-1107476.

References

Bridges, T. J. & Dias, F. 2007 Enhancement of the Benjamin-Feir instability

with dissipation. *Physics of Fluids* **19**, 104104.

Carter, J. D. 2001 Stability and existence of traveling wave solutions of the two-dimensional nonlinear Schrödinger equation and its higher-order generalizations. PhD thesis, University of Colorado at Boulder.

Carter, J. D. & Contreras, C. C. 2008 Stability of plane-wave solutions of a dissipative generalization of the nonlinear Schrödinger equation. *Physica D* **237**, 2392–2396.

Coddington, E. A. & Levinson, N. 1955 *Theory of Ordinary Differential Equations*. McGraw-Hill, New York.

Dias, F., Dyachenko, A. I. & Zakharov, V. E. 2008 Theory of weakly damped free-surface flows: A new formulation based on potential flow solutions. *Physics Letters A* **372**, 1297–1302.

Dysthe, K. B. 1979 Note on a modification to the nonlinear Schrödinger equation for application to deep water waves. *Proceedings of the Royal Society of London A* **369**, 105–114.

Gramstad, O. & Trulsen, K. 2011 Hamiltonian form of the modified nonlinear Schrödinger equation for gravity waves on arbitrary depth. *Journal of Fluid Mechanics* **670**, 404–426.

Hara, T. & Mei, C. C. 1991 Frequency downshift in narrow banded surface waves under the influence of wind. *Journal of Fluid Mechanics* **230**, 429–477.

Islas, A. & Schober, C. M. 2011 Rogue waves and downshifting in the presence of damping. *Natural Hazards and Earth System Sciences* **11**, 383–399.

Kato, Y. & Oikawa, M. 1995 Wave number downshift in modulated wavetrain through a nonlinear damping effect. *Journal of the Physical Society of Japan* **64**, 4660–4669.

Lake, B. M. & Yuen, H. C. 1977 A note on some nonlinear water-wave experiments and the comparison of data with theory. *Journal of Fluid Mechanics* **83**, 75–81.

Lake, B. M., Yuen, H. C., Rungaldier, H. & Ferguson, W. E. 1977 Nonlinear deep water waves: theory and experiment. Part 2. Evolution of a continuous wave train. *Journal of Fluid Mechanics* **83**, 49–74.

Lo, E. & Mei, C. C. 1985 A numerical study of water-wave modulation based on a higher-order nonlinear Schrödinger equation. *Journal of Fluid Mechanics* **150**, 395–416.

Melville, W. K. 1982 The instability and breaking of deep-water waves. *Journal of Fluid Mechanics* **115**, 165–185.

Segur, H., Henderson, D., Carter, J. D., Hammack, J., Li, C., Pheiff, D. & Socha, K. 2005*a* Stabilizing the Benjamin-Feir instability. *Journal of Fluid Mechanics* **539**, 229–271.

Segur, H., Henderson, D. M. & Hammack, J. L 2005*b* Can the Benjamin-Feir instability spawn a rogue wave? In *Proceedings of the 14th 'Aha Huliko'a Hawaiian Winter Workshop Honolulu, Hawaii* (ed. P. Müller & D. M. Henderson), pp. 43–57.

Su, M. Y., Bergin, M., Marler, P. & Myrick, R. 1982 Experiments on nonlinear instabilities and evolution of steep gravity-wave trains. *Journal of Fluid Mechanics* **124**, 45–72.

Trulsen, K. & Dysthe, K. B. 1990 Frequency down-shift through self modulation and breaking. In *NATO ASI Series 178*, pp. 561–572.

Trulsen, K. & Dysthe, K. B. 1997 Frequency downshift in three-dimensional wave trains in a deep basin. *Journal of Fluid Mechanics* **352**, 359–373.

Zakharov, V. E. 1968 Stability of periodic waves of finite amplitude on the surface of a deep fluid. *Journal of Applied Mechanics and Technical Physics* **9** (2), 190–194.